Radiocarbon, Vol 58, Nr 1, 2016, p 193–203 DOI:10.1017/RDC.2015.20

A CASE STUDY USING ^{10}BE-^{26}AL EXPOSURE DATING AT THE XI'AN AMS CENTER

Li Zhang[1,2] • Zhenkun Wu[1,2] • Hong Chang[1] • Ming Li[1,2] • Guocheng Dong[1,2] • Yunchong Fu[1,2] • Guoqing Zhao[1,2] • Weijian Zhou[1,2,3]*

[1]State Key Laboratory of Loess and Quaternary Geology, Institute of Earth Environment, Chinese Academy of Sciences, Xi'an 710061, China.
[2]Shaanxi Key Laboratory of Accelerator Mass Spectrometry Technology and Application, Xi'an AMS Center, Xi'an 710061, China.
[3]Xi'an Jiaotong University, Xi'an 710049, China.

ABSTRACT. Exposure age dating using *in situ* ^{10}Be and ^{26}Al is a very useful technique for dating fluvial terraces. This is especially true in semiarid regions where other methods suffer from a paucity of suitable dating materials. This article describes sample preparation procedures and analytical benchmarks established at the Xi'an Accelerator Mass Spectrometry (AMS) Center for the study of *in situ* ^{10}Be and ^{26}Al. Four intercomparison samples were analyzed in the study, using an improved sample preparation method. The exposure age results are shown to be in good agreement with published data, and demonstrate the reliability of the dating method. This article also presents new ^{10}Be and ^{26}Al results from quartz samples collected from a series of fluvial terraces from Guanshan River, along the Qilian Shan, northeastern Tibetan Plateau. The ages of three fluvial terraces from the Jinfosi site are shown to be (56.4 ± 5.3) ka for T3, (10.7 ± 1.0) ka for T2, and (7.2 ± 1.0) ka for T1. The dating results are consistent with published data from the same region (^{10}Be, ^{14}C, and optically stimulated luminescence dating methods). A comparison of high-resolution climate records with age constraints for the terrace formation shows a close relationship between terrace formation and climate change.

KEYWORDS: ^{10}Be-^{26}Al exposure dating, fluvial terraces, Xi'an AMS, Qilian Shan.

INTRODUCTION

Fluvial terraces can serve as an ideal recorder of climate change and tectonic movement (Schumm 1977). In order to unravel the formation and external controls on such terraces, precise dating is required to determine the timing of terrace formation (Repka et al. 1997). Generally, however, it is difficult to date the depositional sediments on fluvial terraces in semiarid regions because of the paucity of organic materials for ^{14}C dating in such areas (e.g. the Qilian Mountains, northeastern Tibetan Plateau). The common techniques of ^{14}C and optically stimulated luminescence (OSL) may also be limited by their respective time ranges (Brauer et al. 2014). U/Th dating of carbonate coatings on fluvial deposits can sometimes be used successfully to constrain the timing of fluvial terraces (Kelly et al. 2000; Schulte et al. 2008); however, the time lag of coating development is difficult to quantify. Fortunately, developments in cosmogenic radionuclide surface exposure dating have overcome these various limitations (Cockburn 2004).

Sediment-capped alluvial fan surfaces are ideal for exposure dating (Granger et al. 2013). ^{10}Be and ^{26}Al surface exposure dating has been widely used in defining the timing of fluvial terraces (Hancock et al. 1999; Bookhagen et al. 2006; Perrineau et al. 2011; Rixhon et al. 2011). However, studies on ^{10}Be environmental tracer and exposure dating have lagged behind in China due to a lack of accelerator mass spectrometry (AMS) facilities for routine ^{10}Be measurements. It was not until 2006 that the Xi'an AMS Center acquired a 3MV Tandetron-based multielement (^{10}Be, ^{14}C, ^{26}Al, and ^{129}I) AMS. This AMS facility features excellent ^{10}Be detection sensitivity (up to 10^{-15}), and high precision (better than 1.4% at 10^{-12} and 1.14% at 10^{-11}, respectively) for ^{10}Be and ^{26}Al (Zhou et al. 2007). These instrumental capabilities require complementary chemical processing procedures to meet the needs of surface exposure dating studies of fluvial terraces on a large scale. The key steps to reliable ^{10}Be and ^{26}Al exposure ages include sample collection and preparation (pure quartz extraction, and

*Corresponding author. Email: weijian@loess.llqg.ac.cn.

quantitative Be and Al separation). At present, the international community has developed a standardized sampling method (Gosse and Phillips 2001). To extract pure quartz from a rock sample, most procedures are based on the classical method established by Kohl and Nishiizumi (1992). For the separation and extraction of Be and Al, there exist small differences between laboratories (Ivy-Ochs 1996; Schnabel et al. 2007; Akçar et al. 2012; Zheng et al. 2014).

This article presents a comprehensive AMS dating method for fluvial terrace samples from arid regions. We evaluate the analytical reliability of our dating results, and apply them to fluvial terraces from the Qilian Shan. We then discuss the relationship between terrace formation and climate change for this site.

SAMPLING AND DEVELOPMENT OF A ^{10}BE-^{26}AL EXPOSURE DATING METHODOLOGY

Sampling

Our sampling focused on the fluvial terraces along the Guanshan River, located in a central portion of the Fodongmiao-Hongyazi fault zone, near Jinfosi, at the northern margin of the Qilian Shan. Three prominent terraces (T1, T2, and T3) were identified in the field (Figure 1). All three of the terraces are strath terraces composed of gravel and silt. The degree of solidification is relatively high in the higher terraces, as compared with the lower ones, while the proportion of boulders is constant. The terraces form well-preserved planar surfaces. Terrace surfaces are covered with sparse vegetation. There are few boulders exposed on the surface and exhibit low roundness. The samples were chosen with regard to the desired target element quartz. Therefore, we mainly collected quartzites, granites, and gneisses from the terraces. We sampled the upper parts of single boulders that were partly embedded in the deposits to avoid the potential problem of transport after the terrace formation. The thickness of each sample was less than 5 cm. A GPS unit was used to record sample locations and altitudes (Table 1). Shielding from surrounding mountain slopes and dip angles of the samples sites were measured with a clinometer to determine the topographic shielding factor. Based on the principles above, we collected four boulder samples from the focus site in total (Figure 1). JFS-1-8 was collected from a biotite adamellite boulder on the surface of T1. JFS and JFS-1-3 were sampled from T2. Sample JFS-1-2 came from a granitic rock imbedded in the surface of T3.

Method

Optimization of the Experimental Procedure

Samples collected from the field were cleaned, dried, and crushed. The 0.25–0.50-mm fractions were isolated using standard testing sieves. Magnetic separation was used to remove magnetic minerals. Then, aluminosilicate minerals, such as feldspar, along with meteoric ^{10}Be were removed by 4–5 iterations of acid leaching at 100°C on a hotdog roller using a mixed solution of dilute HF and HNO_3 (Kohl and Nishiizumi 1992). Pure quartz samples were completely dissolved with 0.3–0.5 mg ^{9}Be carrier in hydrofluoric acid. Fluorides were removed by perchloric acid fuming. Beryllium and aluminum were separated by cation and anion exchange chromatography, and leached with 1 mol/L HCl and an $H_2C_2O_4$-HCl acid mixture. Ammonium hydroxide was added to the ^{10}Be and ^{26}Al fractions to precipitate beryllium and aluminum hydroxide gels at pH = 8–9 and pH = 8, respectively, and the hydroxides were oxidized by ignition at 900°C in quartz crucibles (Figure 2a). The beryllium oxide and aluminum oxide products were mixed with copper powder and pressed into target holders prior to measurement on the AMS.

https://doi.org/10.1017/RDC.2015.20 Published online by Cambridge University Press

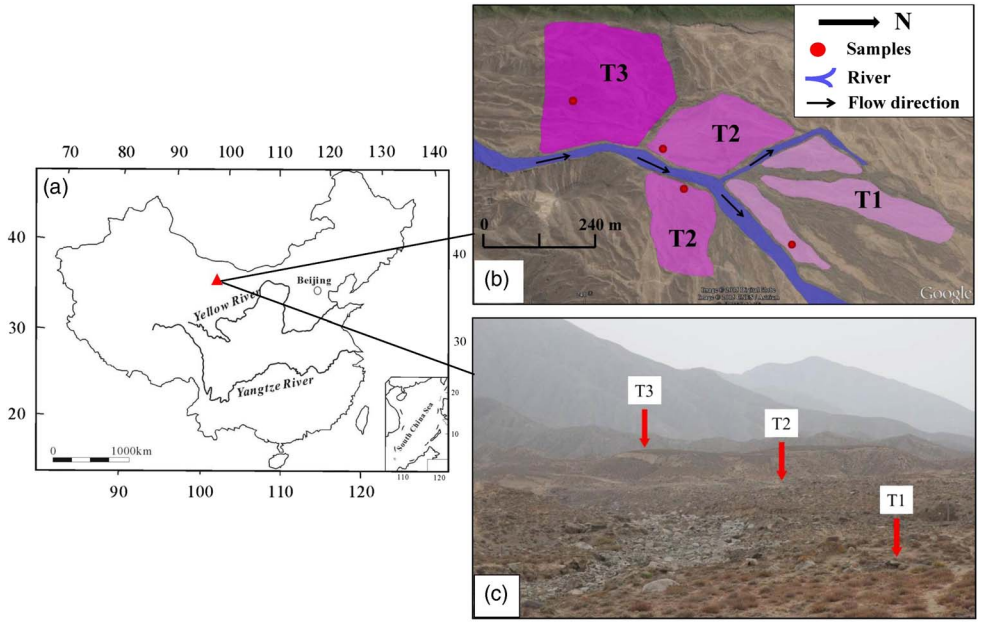

Figure 1 (a) Map of China showing the sampling site; (b) Google Earth image of the sampling site identified in (a). T1, T2, and T3 represent terraces 1, 2, and 3, respectively; (c) southwest view of the terraces.

Table 1 Dating results of Jinfosi terraces using ^{10}Be and ^{26}Al surface exposure ages.

Sample No.	Location	Latitude (°N)	Longitude (°E)	Elevation (m asl)	Thickness (cm)	Shielding correction	^{10}Be concentration (10^5 atoms/g)	^{26}Al concentration (10^5 atoms/g)	^{10}Be age (ka)	^{26}Al age (ka)
JFS-1-8	T1	39.4334	98.6942	1754	3.7	0.9988	1.14 ± 0.12	5.00 ± 1.43	7.3 ± 1.0	4.6 ± 1.4
JFS-1-8	T1	39.4334	98.6942	1754	3.0	0.9988	1.11 ± 0.15	5.38 ± 1.81	7.1 ± 1.1	4.9 ± 1.7
JFS-1-3	T2	39.4307	98.6915	1803	5.0	0.9977	0.69 ± 0.05	4.05 ± 0.16	4.3 ± 0.5	3.6 ± 0.3
JFS	T2	39.4311	98.6926	1795	5.0	1	1.70 ± 0.05	10.90 ± 0.65	10.7 ± 1.0	9.8 ± 1.0
JFS-1-2	T3	39.4289	98.6902	1837	3.5	0.9942	9.14 ± 0.30	57.86 ± 1.97	56.4 ± 5.3	51.1 ± 4.9

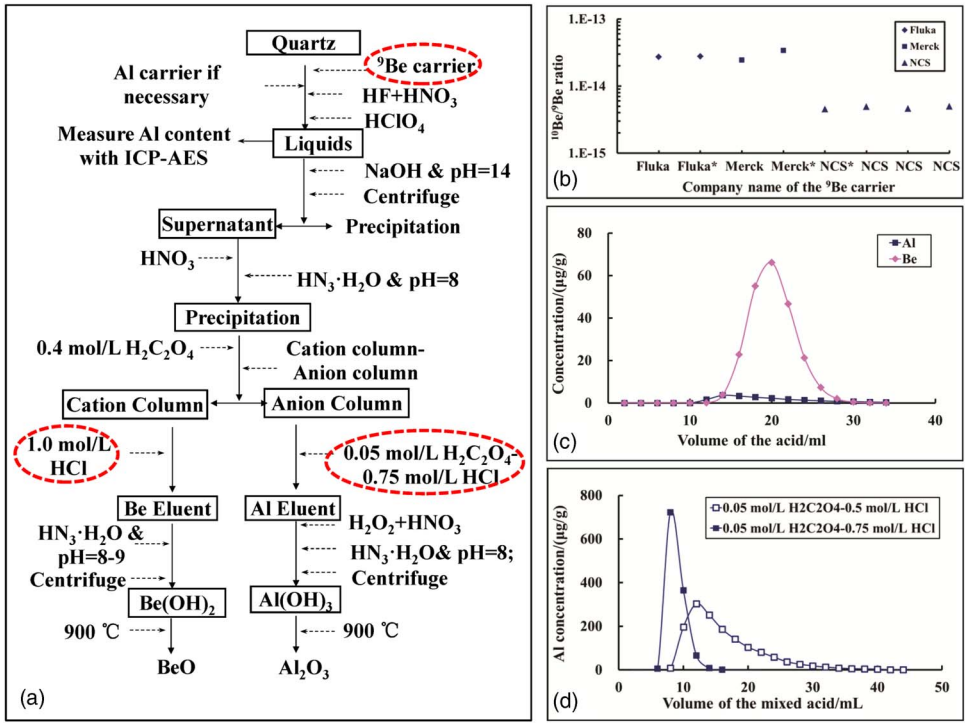

Figure 2 (a) Experimental procedure of Be and Al extraction from pure quartz; (b) ^{10}Be/^{9}Be ratio of ^{9}Be carriers from different companies (*: data from Zhang et al. 2012); (c) leaching curves of the cation exchange resin column with 1.0 mol/L HCl; (d) leaching curves of the anion exchange resin column with different concentrations of $H_2C_2O_4$–HCl mixed solutions.

Based on previous results (Zhang et al. 2012), a series of experiments was devised to optimize the separation and recovery of Be and Al. This included the selection of a ^{9}Be carrier and proper acid concentrations for anion and cation exchange (Figure 2a).

In order to test the elution efficiency, we designed a stepwise experiment that included inductively coupled plasma-atomic emission spectrometry (ICP-AES) measurements of Be and Al concentrations in successive solutions. Solutions were eluted from cation and anion exchange resin columns with HCl and $H_2C_2O_4$–HCl mixtures. The leachate was collected for each step and put into numbered centrifuge bottles. For Be^{2+} solutions, a concentration of 1 mol/L HCl was found to be relatively ideal (Figure 2c), with a recovery rate more than 98%. However, when using a 0.05 mol/L $H_2C_2O_4$–0.50 mol/L HCl acid mixture to elute Al^{3+}, we observed unacceptably high peak tailing (tailing factor ~2.75) in the leaching profile (Figure 2d). Since the distribution coefficient of Al varies with different mixtures of these two acids, we were able to overcome this shortfall by using a 0.05 mol/L $H_2C_2O_4$–0.75 mol/L HCl acid mixture. With the higher HCl concentration, the Al elution curve does not show the tailing (Figure 2d) and the recovery rate is more than 80%.

A low ^{10}Be/^{9}Be carrier is critical for the measurement of samples with low ^{10}Be concentrations or small weight. We analyzed several commercial ^{9}Be carriers, using 0.5-mL aliquots. These were produced by Fluka (catalog number: GA19094, lot number: 1318495 51508286), Merck (catalog number: UN3264, lot number: HC825289), and NCS (catalog number: GSB G 62002-90(0402), lot number: 10011832). As shown in Figure 2b, the results can be divided into two

https://doi.org/10.1017/RDC.2015.20 Published online by Cambridge University Press

groups. The first one (Fluka and Merck carriers) is at the 10^{-14} level and similar to published data measured at ASTER and Gif (Merchel et al. 2008). The second one (NCS carrier) is found to have a ^{10}Be/^{9}Be ratio of about one magnitude lower than the other two. Thus, we chose the NCS ^{9}Be carrier in our study.

Results and Reliability of the Method

In order to test the reliability of our method, four intercomparison samples (two quartz samples and two sand samples) were analyzed. The quartz samples (Sample A and Sample N) are intercomparison samples from the CRONUS-Earth Project, provided by Dr Tim Jull, University of Arizona. These samples were distributed to several laboratories in the USA, UK, France, Switzerland, Germany, the Netherlands, Sweden, Australia, and Canada (Jull et al. 2015). The sand samples (JWS10-09 and JWS10-10) were collected from Minjiang River in 2009 and 2010 by Joshua A West, University of Southern California, Los Angeles (West et al. 2014).

The respective ^{10}Be and ^{26}Al mean concentrations of Sample A are $(3.42 \pm 0.10) \times 10^{7}$ atoms/g and $(1.43 \pm 0.07) \times 10^{8}$ atoms/g. The ^{10}Be and ^{26}Al mean concentrations of Sample N are $(2.17 \pm 0.09) \times 10^{5}$ atoms/g and $(1.05 \pm 0.11) \times 10^{6}$ atoms/g, respectively (Jull et al. 2015). The ^{10}Be results are compared with those of 12 laboratories, while the ^{26}Al data are compared with the ones provided by six (Sample A) and five (Sample N) laboratories (Figure 3). The mean values of data from the other laboratories are shown at the 1σ level. The results show that the data at the Xi'an AMS Center agree well with the values reported by other labs (Jull et al. 2015). The ^{10}Be concentration of JWS10-09 and JWS10-10 are $(3.17 \pm 0.22) \times 10^{4}$ atoms/g and $(3.14 \pm 0.22) \times 10^{4}$ atoms/g, respectively. To account for the fact that the standards used were different from each other, our data were normalized to the same as that of West et al. (2014).

In summary, the previous experimental procedures were optimized for the ^{9}Be carrier chosen and the leaching acid concentrations for the Be and Al extraction with anion and cation exchange resins. The intercomparison experiments verify the sample preparation and AMS protocols applied here.

The next step was to use our methodology to process a set of fluvial terrace samples. The total Al concentrations of dissolved quartz samples from the terraces were quantified by inductively coupled plasma-atomic emission spectrometry (ICP-AES) at the Institute of Earth Environment, Chinese Academy of Sciences, and the ^{10}Be and ^{26}Al concentrations were measured with the 3MV AMS at the Xi'an AMS Center (Zhou et al. 2007). The ^{10}Be/^{9}Be ratios of the samples were normalized to the NIST AMS standard SRM-4325 with a nominal value of ^{10}Be/^{9}Be = 2.68×10^{-11} (Nishiizumi et al. 2007). The ^{26}Al/^{27}Al ratios of the samples were normalized to the ICN AMS standard with a nominal value of ^{26}Al/^{27}Al = 1.065×10^{-11} (Nishiizumi et al. 2007).

RESULTS AND DISCUSSION

Dating Results of the Fluvial Terraces

The fluvial-terrace sample results are presented in Table 1. After we measured the ^{10}Be and ^{26}Al concentrations of the samples, we calculated the exposure ages following the formula

$$t = -\frac{1}{\lambda + \mu\epsilon} \ln\left(1 - \frac{N}{P}(\lambda + \mu\epsilon)\right)$$

where λ is the decay constant (1/yr, $\lambda_{10Be} = 4.998 \times 10^{-7}$, $\lambda_{26Al} = 9.87 \times 10^{-7}$), μ is the cosmic-ray attenuation coefficient ($\mu = \rho/L$: $L = 160$ g/cm^2 and ρ is the density of the rock), ε is the erosion rate, P is the production rate of the nuclide at the surface (atoms/g/yr), and N is

https://doi.org/10.1017/RDC.2015.20 Published online by Cambridge University Press

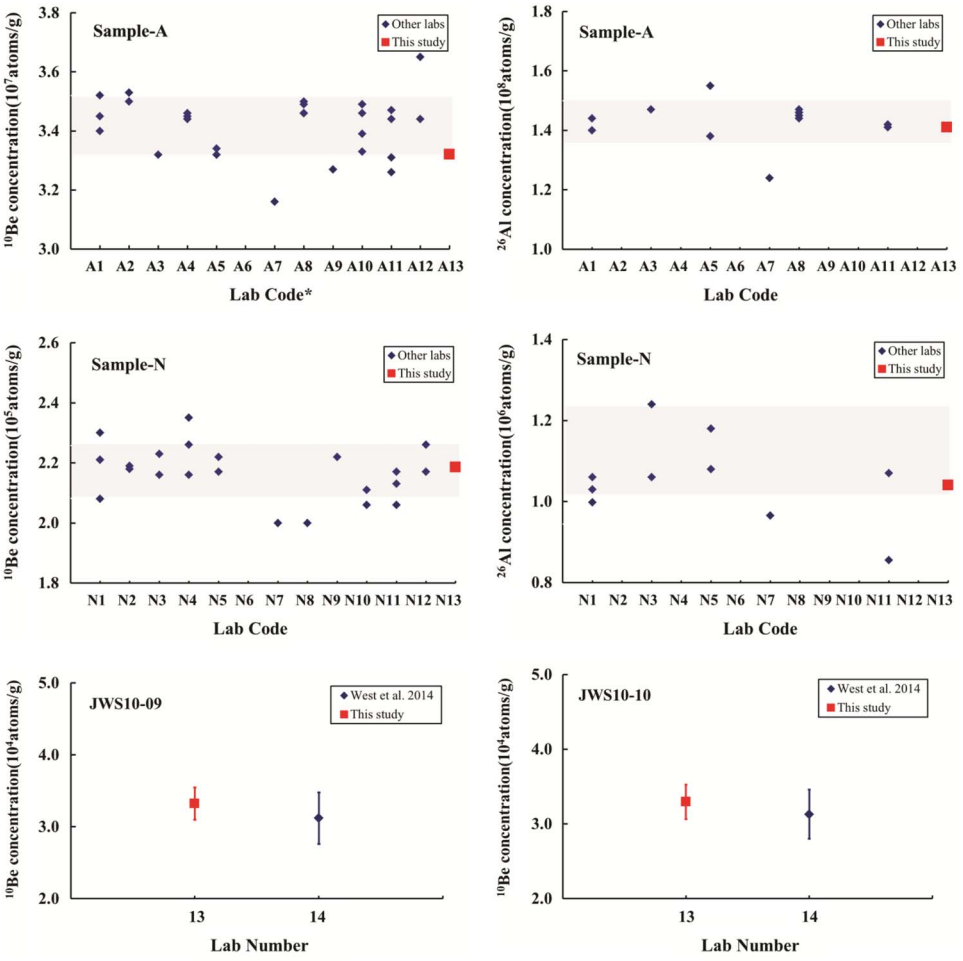

Figure 3 Results of the intercomparison samples (West et al. 2014; Jull et al. 2015). Lab code: letter identifies the sample, number identifies the laboratory (13 is this study). The shaded part is the mean value of published data with standard deviation. Only ^{10}Be data are plotted for JWS10-09 and JWS10-10 because ^{26}Al data from Lab 14 were unavailable.

the concentration of the nuclide (atoms/g). To calculate exposure ages, we used a sea-level, high-latitude production rate of 4.76 atoms/g/yr for ^{10}Be and 30.6 atoms/g/yr for ^{26}Al (Balco 2008, 2009). The production rates were scaled to the location of the sampling site with the scaling scheme of Lal (1991) and Stone (2000). All ages have been calculated assuming no erosion.

Ages obtained by both ^{10}Be and ^{26}Al are reasonably consistent, but the ^{26}Al ages appear to be systematically younger (Table 1). We plot our results on a standard ^{26}Al/^{10}Be vs. ^{10}Be plot (Figure 4). It shows that JFS and JFS-1-2 are outside but near the steady-state erosion island, while JFS-1-3 lays under the erosion island. The two results of JFS-1-8 are also near the erosion island but with larger uncertainties. In general, we tend to have more confidence in the ^{10}Be ages, as they require only one measurement, ^{10}Be/^{9}Be, while ^{26}Al requires measurement of both ^{26}Al/^{27}Al and Al concentration (van der Woerd et al. 2006). Therefore, the following discussion is framed around only the ^{10}Be data.

https://doi.org/10.1017/RDC.2015.20 Published online by Cambridge University Press

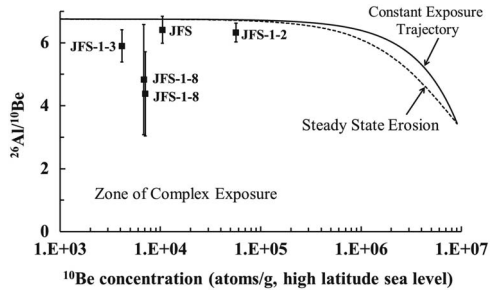

Figure 4 Diagram of the ^{26}Al/^{10}Be ratios vs. ^{10}Be concentrations for Guanshan River samples.

There are significant differences among samples JFS-1-3 and JFS, which were both collected from T2, although the preparation of both samples presented no irregularities. The quality of a surface exposure age determined from a single geomorphic feature is often difficult to assess in the absence of independent geological age constraints (Hetzel et al. 2002). Investigating a series of fluvial terraces has the advantage that the relative age of the terraces is unequivocally determined, i.e. higher terraces are older than lower terraces. In accord with the age of T1 (7.3 ± 1.0 and 7.1 ± 1.1 ka), the formation of T2 is best represented by the age of sample JFS. According to Owen et al. (2003), there are two factors that dominate the potential variability in boulder ages in the Qilian Shan: (1) severe weathering and (2) shielding due to the development of a thick organic turf and sporadic deposits of loess. We were particularly careful to sample only from boulders that did not show evidence of significant weathering. However, although the JFS and JFS-1-3 are from the same terrace, collected at different dates, the results are not consistent. We explain that the weathering and burial histories of JFS-1-3 are not clear. The process might result in an underestimated age. Therefore, we reject the dating result of JFS-1-3. For JFS-1-8, we use the average of the two results (7.2 ± 1.0 ka) determined to represent the age of T1.

The ages we determined are abandonment ages, which date to the time when stream incision began. Based on the earlier discussion, we chose the ^{10}Be ages to represent the ages of the terraces. Our chronology suggests that the terraces T1, T2, and T3 were abandoned at 56.4 ± 5.3, 10.7 ± 1.0, and 7.2 ± 1.0 ka, respectively. The calculated ^{10}Be exposure ages shown in Table 1 are consistent with the stratigraphic sequences, that is, decreasing in age from the uppermost terrace to the lowermost terrace. This correspondence supports our use of cosmogenic nuclide exposure dating for the Qilian Shan fluvial terraces.

Comparison with Published Data of the Fluvial Terraces in the Arid Region of China

Our results also show good agreement with published data from fluvial terraces from several arid regions in China (Table 2).

River Incision Rate

River incision rates can be calculated from the height and age difference between successive terraces (Gu et al. 2006). With the small data set we collected here, we can make a preliminary estimate for the incision rate of Guanshan River. Taking the ^{10}Be ages for T3 (56.4 ± 5.3 ka) and T2 (10.7 ± 1.0 ka) and combining them with the elevation difference of 38 m between the two terraces, we calculate an incision rate of about 0.8 mm/yr. Using the lower error limit for T3

https://doi.org/10.1017/RDC.2015.20 Published online by Cambridge University Press

Table 2 Comparison of the formation age of terraces in arid regions of China.

	Age (ka)				
Sample location	T3	T2	T1	Dating method	Reference
Qilian Shan Jinfosi	56.4	10.7	7.2	^{10}Be	This study
Altyn Tagh Aksay&Bangguoba	55.8	11.9	6.8	^{10}Be	Mériaux et al. 2005
Altyn Tagh Huermo&Cherchen	60.6	10	7.3	^{10}Be	Mériaux et al. 2004, 2005
Yumen Shiyouhe	61	10.9		^{10}Be	Hetzel et al. 2006
Riyueshan		10.1	7.2	^{14}C	Yuan et al. 2011
Riyueshan		10.9		OSL	Yuan et al. 2011

(51.1 ka) and a conservative upper age limit for T2 of 11.7 ka gives a maximum incision rate of about 1 mm/yr in the late Pleistocene for Guanshan River, which is in good agreement with that of the Shiyou River (a very close area) (Hetzel et al. 2006). In contrast, the ^{10}Be age of T1 (7.2 ± 1.0 ka), which is located 45 m lower than T2, suggests that during the Holocene the river incised at an average rate of 13 mm/yr. Even if we use the upper error limit of the ^{10}Be age of 11.7 ka for T2 and the lower error limit of the ^{10}Be age of 6.2 ka for T1, the resulting incision rate of 8 mm/yr is still about seven times higher than the maximum rate of about 1 mm/yr for the late Pleistocene. Based on the calculation above, the age of T2 marks the onset a remarkable period of incision of the Guanshan River. Hetzel et al. (2006) reported that the Shiyou River incision accelerated from (0.8 ± 0.2) mm/yr to 10 mm/yr at 10–15 ka. Our preliminary estimate is similar to theirs, and points to the need for further study to understand the nature of this dramatic increase in incision rate.

Timing of Terrace Formation and Past Climate Change

Chen (2003) considered climate change as the key factor that caused the deposition of terraces and subsequent river incision over a large region along the Hexi Corridor. To assess the role of climate in the Qilian Shan, we compare our age data with a record of Marine Isotope Stages (MIS) (Lisiecki and Raymo 2005) (Figure 5). The age of T3 corresponds with MIS3 (57–29 ka BP). Stage 3 is usually called an interstadial. In the Guliya ice-core record, however, the temperature during stage 3 was higher than today and relatively warm and wet (Yao et al. 1997). The same trend is observed from loess-paleosol sequences on the Loess Plateau (Kuhle 1998), and from pollen records from the southern margin of the Tibetan Plateau, in Ladakh, India (Bhattacharyya 1989). Paleolake and paleovegetation studies have also provided evidence for abnormally warm climate at this time. For example, the δ^{18}O and sedimentological records from core TS95 from Tianshuihai Lake, in the Qinghai region of the Tibetan Plateau, also indicate the presence of high lake levels during 59–56 ka. Thus, Li et al. (2008) attributed increased meltwater, due to climate warming, to be the cause of high lake level events during this time.

The age of T2 corresponds with MIS1. The beginning of MIS1 is marked by significant climatic warming associated with dramatic increases in meltwater as well as rainfall. The increased water flow may be expected to enhance erosion and initiate river incision and hence the formation of T2. The incision of T1 occurs during the Holocene climate optimum, characterized by a warm and wet period between 6–8 ka. Stratigraphic and chronological studies from the Hongshui River section, in the southern portion of the Tengger Desert, have been used to reconstruct paleoclimatic changes during 3–8 ka by Zhang et al. (1999). They observe an increase in humidity at this time. Increased precipitation and glacial

https://doi.org/10.1017/RDC.2015.20 Published online by Cambridge University Press

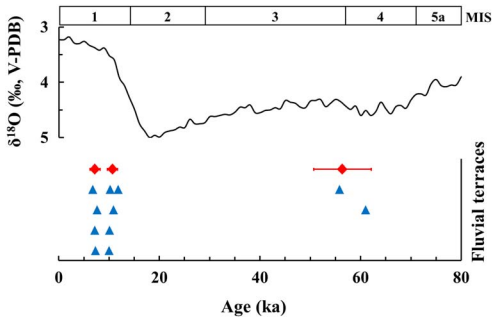

Figure 5 Comparison of formation age of fluvial terraces with Marine Isotope Stages (Lisiecki and Raymo 2005). Ages with red diamonds correspond to our ^{10}Be results with 1σ uncertainties. Ages with blue triangles correspond to published data from other fluvial terraces (Lasserre et al. 1999; Mériaux et al. 2004, 2005; Hetzel et al. 2006; Yuan et al. 2011).

melting caused increased stream discharge that enhanced fluvial incision and abandonment of the terraces.

In summary, a comparison of high-resolution climate records with age constraints for terrace formation reflects the close relationship between terrace formation and climate change. Apart from tectonic movement, climate change can significantly influence the river incision and terrace formation over a large region.

CONCLUSIONS

The results of four intercomparison samples show that the exposure dating method described here, for the Xi'an AMS Center, are in good agreement with published data, and provide reliable results for cosmogenic exposure age studies. Exposure ages of three fluvial terraces from the Qilian Shan were determined using ^{10}Be and ^{26}Al and are shown to be in good agreement with published data supporting a strong climatic role in the development of the terraces. The methodology described herein can support a wide range of applications in the study of fluvial terrace development in arid regions.

ACKNOWLEDGEMENTS

This work was jointly supported by the Ministry of Science and Technology of China, National Science Foundation of China, and Chinese Academy of Sciences. We especially thank Prof Guanjun Shen for his valuable assistance in chemical treatment; Prof George S Burr for English improvement; Dr Huiping Zhang for assistance in field sampling; Prof Tim Jull, Zhangdong Jin, and Dr Joshua A West for providing the intercomparison samples; and Xiaohu Xiong for assistance in the ICP-AES measurements. We thank the editor and the two reviewers for their constructive comments and suggestions.

REFERENCES

Akçar N, Deline P, Ivy-Ochs S, Alflmov A, Hajdas I, Kubik PW, Christl M, Schlüchter C. 2012. The AD 1717 rock avalanche deposits in the upper Ferret Valley (Italy): a dating approach with cosmogenic ^{10}Be. *Journal of Quaternary Science* 27(4):383–92.

Balco G. 2008. A complete and easily accessible means of calculating surface exposure ages or

https://doi.org/10.1017/RDC.2015.20 Published online by Cambridge University Press

erosion rates from ^{10}Be and ^{26}Al measurements. *Quaternary Geochronology* 3:174–95.

Balco G. 2009. ^{26}Al-^{10}Be exposure age/erosion rate calculators: update from v.2.1 to v.2.2. http://hess.ess.washington.edu/math/.

Bhattacharyya A. 1989. Vegetation and climate during the last 30,000 years in Ladakh. *Palaeogeography, Palaeoclimatology, Palaeoecology* 73(1–2):25–38.

Bookhagen B, Fleitmann D, Nishiizumi K, Strecker MR, Thiede RC. 2006. Holocene monsoonal dynamics and fluvial terrace formation in the northwest Himalaya, India. *Geology* 34(7):601–4.

Brauer A, Hajdas I, Blockley SP, Bronk Ramsey C, Christl M, Ivy-Ochs S, Moseleye GE, Nowaczyka NN, Rasmussenf SO, Robertsg HM, Spötle C, Staffd RA, Svensson A. 2014. The importance of independent chronology in integrating records of past climate change for the 60–8 ka INTIMATE time interval. *Quaternary Science Reviews* 106: 47–66.

Chen WB. 2003. Principal features of tectonic deformation and their generation mechanism in the Hexi Corridor and its adjacent regions since late Quaternary [PhD dissertation]. Institute of Geology, China Seismological Bureau. p 56–9.

Cockburn HAP. 2004. Geomorphological applications of cosmogenic isotope analysis. *Progress in Physical Geography* 28(1):1–42.

Gosse JC, Phillips FM. 2001. Terrestrial in situ cosmogenic nuclides: theory and application. *Quaternary Science Reviews* 20(14):1475–560.

Granger DE, Lifton NA, Willenbring JK. 2013. A cosmic trip: 25 years of cosmogenic nuclides in geology. *Geological Society of America Bulletin* 125(9–10):1379–402.

Gu ZY, Xu B, Lv YW, Aldahan A, Lal D. 2006. A report on ^{10}Be dating of terrace surfaces in Nujiang Riser Valley. *Quaternary Sciences* 26(2):293–4. In Chinese.

Hancock GS, Anderson RS, Chadwick OA, Finkel RC. 1999. Dating fluvial terraces with ^{10}Be and ^{26}Al profiles: application to the Wind River, Wyoming. *Geomorphology* 27(1–2):41–60.

Hetzel R, Niedermann S, Ivy-Ochs S, Kubik PW, Tao MX, Gao B. 2002. ^{21}Ne versus ^{10}Be and ^{26}Al exposure ages of fluvial terraces: the influence of crustal Ne in quartz. *Earth and Planetary Science Letters* 201(3):575–91.

Hetzel R, Niedermann S, Tao MX, Kubik PW, Strecker MR. 2006. Climatic versus tectonic control on river incision at the margin of NE Tibet: ^{10}Be exposure dating of river terraces at the mountain front of the Qilian Shan. *Journal of Geophysical Research* 111:F03012.

Ivy-Ochs S. 1996. The dating of rock surfaces using *in situ* produced ^{10}Be, ^{26}Al and ^{36}Cl, with examples from Antarctica and the Swiss Alps [PhD dissertation]. Zurich: ETH.

Jull AJT, Scott EM, Bierman P. 2015. The CRONUS-Earth inter-comparison for cosmogenic isotope analysis. *Quaternary Geochronology* 26: 3–10.

Kelly M, Black S, Rowan JS. 2000. A calcrete-based U/Th chronology for landform evolution in the Sorbas basin, southeast Spain. *Quaternary Science Reviews* 19(10):995–1010.

Kohl CP, Nishiizumi K. 1992. Chemical isolation of quartz for measurement of *in-situ*-produced cosmogenic nuclides. *Geochimica et Cosmochimica Acta* 56(9):3583–7.

Kuhle M. 1998. Reconstruction of the 2.4 million km^2 late Pleistocene ice sheet on the Tibetan Plateau and its impact on the global climate. *Quaternary International* 45–46:71–108.

Lal D. 1991. Cosmic ray labeling of erosion surfaces: in situ nuclide production rates and erosion models. *Earth and Planetary Science Letters* 104(2–4): 424–39.

Lasserre P, Morel PH, Gaudemer Y, Tapponnier P, Ryerson FJ, King GCP, Metivier F, Kasser M, Kashgarian M, Liu BC, Lu TY, Yuan DY. 1999. Postglacial left slip rate and past occurrence of $M \geq 8$ earthquakes on the Western Haiyuan Fault, Gansu, China. *Journal of Geophysical Research: Solid Earth* 104(B8):17,633–51.

Li SJ, Zhang HL, Shi YF, Zhu ZY. 2008. A high resolution MIS3 environmental change record derived from lacustrine deposit of Tianshuihai Lake, Qinghai-Tibet Plateau. *Quaternary Sciences* 28(1):122–31. In Chinese.

Lisiecki LE, Raymo ME. 2005. A Pliocene-Pleistocene stack of 57 globally distributed benthic ^{18}O records. *Paleoceanography* 20: PA1003.

Merchel S, Arnold M, Aumaitre G, Benedetti L, Bourles DL, Braucher R, Alfimov V, Freeman SPHT, Steier P, Wallner A. 2008. Towards more precise ^{10}Be and ^{36}Cl data from measurements at the 10^{-14} level: influence of sample preparation. *Nuclear Instruments and Methods in Physics Research B* 266:4921–6.

Mériaux AS, Ryerson FJ, Tapponnier P. 2004. Rapid slip along the central Altyn Tagh Fault: morphochronologic evidence from Cherchen He and Sulamu Tagh. *Journal of Geophysical Research* 109:B06401.

Mériaux AS, Tapponnier P, Ryerson FJ, Xu XW, King G, van der Woerd J, Finkel RC, Li HB, Caffee MW, Xu ZQ, Chen WB. 2005. The Aksay segment of the northern Altyn Tagh Fault: tectonic geomorphology, landscape evolution, and Holocene slip rate. *Journal of Geophysical Research* 110:B04404.

Nishiizumi K, Imamura M, Caffee MW, Southon JR, Finkel RC, McAninch J. 2007. Absolute calibration of ^{10}Be AMS standards. *Nuclear Instruments and Methods in Physics Research B* 258:403–13.

Owen LA, Spencer JQ, Ma HZ, Barnard RL, Derbyshier E, Finkel RC, Caffee MW, Zeng YN. 2003. Timing of late Quaternary glaciation along

the southwestern slopes of the Qilian Shan, Tibet. *Boreas* 32:281–91.

Perrineau A, van Der Woerd J, Gaudemer Y, Liu-Zeng J, Pik R, Tapponnier P, Thuizat R, Zheng RZ. 2011. Incision rate of the Yellow River in Northeastern Tibet constrained by ^{10}Be and ^{26}Al cosmogenic isotope dating of fluvial terraces: implications for catchment evolution and plateau building. *Geological Society London* 353:189–219.

Repka JL, Anderson RS, Finkel RC. 1997. Cosmogenic dating of fluvial terraces, Fremont River, Utah. *Earth and Planetary Science Letters* 152(1–4):59–73.

Rixhon G, Braucher R, Bourlès D, Siame L, Bovy B, Demoulin A. 2011. Quaternary river incision in NE Ardennes (Belgium)—insights from $^{10}Be/^{26}Al$ dating of river terraces. *Quaternary Geochronology* 6(2):273–84.

Schnabel C, Reinhardt L, Barrows TT, Bishop P, Davidson A, Fifield LK, Freeman S, Kim JY, Maden C, Xu S. 2007. Inter-comparison in ^{10}Be analysis starting from pre-purified quartz. *Nuclear Instruments and Methods in Physics Research B* 259:571–5.

Schulte L, Juliá R, Burjachs F, Hilgers A. 2008. Middle Pleistocene to Holocene geochronology of the River Aguas terrace sequence (Iberian Peninsula): fluvial response to Mediterranean environmental change. *Geomorphology* 98(1–2): 13–33.

Schumm SA. 1977. *The Fluvial System*. Hoboken: John Wiley and Sons.

Stone JO. 2000. Air pressure and cosmogenic isotope production. *Journal of Geophysical Research: Solid Earth* 105(B10):23,753–9.

van der Woerd J, Klinger Y, Kerry Sieh, Tapponnier P, Ryerson FJ, Mériaux A-S. 2006. Long-term slip rate of the southern San Andreas Fault from ^{10}Be-^{26}Al surface exposure dating of an offset alluvial fan. *Journal of Geophysical Research: Solid Earth* 111:B04407.

West AJ, Hetzel R, Li G, Jin ZD, Zhang F, Hilton RG, Densmore AL. 2014. Dilution of ^{10}Be in detrital quartz by earthquake-induced landslides: implications for determining denudation rates and potential to provide insights into landslide sediment dynamics. *Earth and Planetary Science Letters* 396:143–53.

Yao TD, Thompson LG, Shi YF, Jiao KQ, Zhang XP. 1997. A study on the climate changes from Guliya ice core records since Last Interglacial Period. *Science in China (Series D)* 6:447–52.

Yuan DY, Champagnac JD, Ge WP, Molnar P, Zhang PZ, Zheng WJ, Zhang HP, Liu XW. 2011. Late Quaternary right-lateral slip rates of faults adjacent to the lake Qinghai, northeastern margin of the Tibetan Plateau. *Geological Society of America Bulletin* 123(9–10): 2016–30.

Zhang HC, Ma YZ, Li JJ, Pachur HJ, Wuenneman B. 1999. The Holocene palaeoclimatic change in southern vicinity of Tengger Desert. *Chinese Science Bulletin* 44(6):550–5.

Zhang L, Zhou WJ, Chang H, Zhao GQ, Song SH, Wu ZK. 2012. The extraction of in-situ ^{10}Be and ^{26}Al from rock sample and accelerator mass spectrometric measurements. *Rock and Mineral Analysis* 3(1):83–9. In Chinese.

Zheng Y, Jia J, Nie XK, Kong P. 2014. Cosmogenic nuclide burial age of the Sanying Formation and its implications. *Science China: Earth Sciences* 57(6):1141–9.

Zhou WJ, Lu XF, Wu ZK, Zhao WN, Huang CH, Li LL, Cheng P, Xin ZH. 2007. New results on Xi'an-AMS and sample preparation systems at Xi'an-AMS Center. *Nuclear Instruments and Methods in Physics Research B* 262:135–42.

https://doi.org/10.1017/RDC.2015.20 Published online by Cambridge University Press